**Final Technical Report**, "Time resolved electrical, optical, and thermal probes of topological spin textures in magnetic nanostructures," Early Career Award, DE-SC0012245

Program officer: Jane Zhu (Jane.Zhu@science.doe.gov)

PI: Gregory D. Fuchs (gdf9@cornell.edu)
Cornell University

This project is a fundamental study of magnetization dynamics in nanoscale spin textures with topological properties. One example is magnetic skyrmions that form in chiral ferromagnetic material systems that lack inversion symmetry. We have concentrated on the scalable chiral magnetic metal B20 FeGe thin film that has an asymmetric exchange interaction due to non-centrosymmetric cubic lattice. While the asymmetric exchange interaction can be found at the interface of a ferromagnet and a heavy metal, manipulation of skyrmions at these interfaces is non-trivial due to pinning and it requires higher critical current. In contrast, B20 materials such as FeGe have superior material quality to offer pinning-free and low-current skyrmion motion.

## Major Accomplishments:

### *Growth and characterization of thin-film B20 FeGe*

We have successfully grown stoichiometric and [111] ordered FeGe films on Si [111] via low temperature co-sputtering from Fe and Ge targets, followed by annealing. Film thickness between 10 nm and 200 nm have been grown, and they are ordered with respect to the underlying Si substrate. Figure 1(a) shows x-ray diffraction results on a 120 nm FeGe film showing the B20 FeGe [111] peak along with the peak from the underlying Si [111] substrate. Using an x-ray spectrometer with an area detector, we show in Figure 1(b) that not only does the FeGe film have <111> texture in the

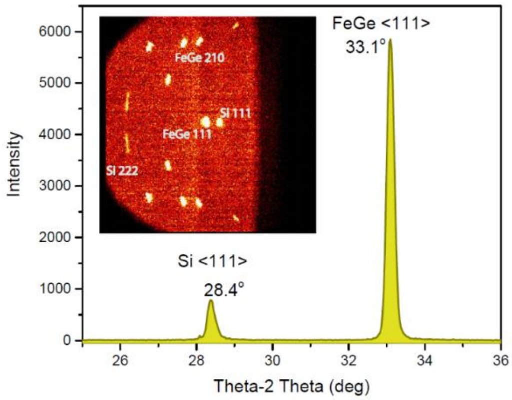

*Figure 1. X-ray diffraction data showing the FeGe[111] peak and the Si [111] substrate peak. Inset: x-ray data taken with a spectrometer equipped with an area detector, showing the mutual orientation among FeGe grains.*

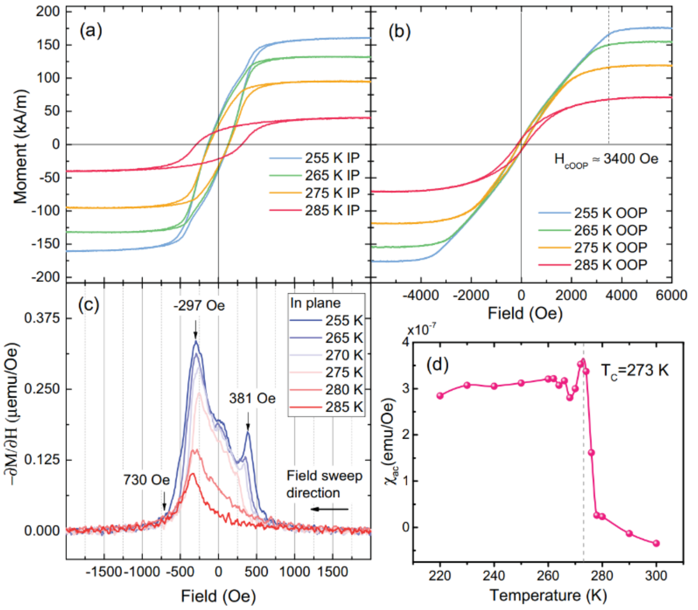

*Figure 2. Magnetometry measurements of our thin film FeGe. (a) M-H curves for the in-plane (IP) and (b) for the OOP fields. (c) The derivative of the IP magnetization with respect to the applied magnetic field to better reveal unwinding of the helical phase. (d) The ac magnetic susceptibility with 20 Oe dc and 10 Oe ac field in the plane.*

growth direction, but the majority of grains have an epitaxial relationship with the substrate.

Bulk magnetic characterization of these films is shown in Figure 2. These results show a magnetic response that is consistent with previous reports of FeGe thin films, including a chiral ordering temperature at T = 273 K as revealed by a peak in the magnetic susceptibility. Likewise, measurements of the magnetic moment as a function of magnetic field and temperature are consistent with previous reports both in terms of the magnitude of the moment and in terms of the magnetic anisotropy. From these measurements, we conclude that we have grown magnetically high-quality B20 FeGe films.

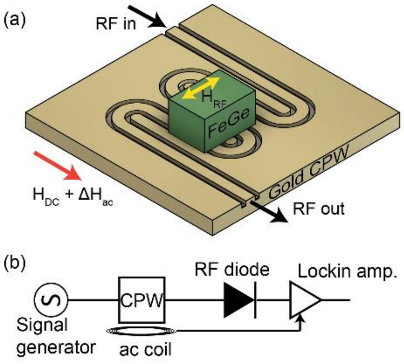

*Figure 3. Schematic of the microwave absorption spectroscopy. (a) The FeGe film is placed on a broadband coplanar waveguide and the absorbed microwave power is monitored as we vary the magnetic field, frequency, and temperature. (b) We lockin to voltage from an RF diode referenced to magnetic field ac modulation.*

### *Chiral magnetic resonance*

After obtaining optimum growth conditions for FeGe thin film by magnetron sputtering, we systematically characterized our films and investigated their chiral magnetic properties using microwave absorption spectroscopy (MAS). In the MAS, illustrated in Figure 3, the FeGe film is placed on a broadband coplanar waveguide to study resonance spin dynamics under application of d.c. and a.c. magnetic fields. At the frequency, field, and temperature of a particular magnetic resonance, microwave power is absorbed from the transmission line and detected in our experiment. By systematically varying these parameters we can locate magnetic resonance and spin-wave resonances in the sample with unparalleled sensitivity and control.

In Figure 4, we show the emergence of a chiral magnetic resonances in the MAS data. While the film shows only very weak microwave absorption in its paramagnetic state at 283 K (Figure 4a), it has a uniform ferromagnetic resonance at 273.5 K – just preceding its chiral ordering temperature of 273 K (Figure 4b). At 258 K (Figure 4c), we observe an additional resonance feature from the helical phase (arrow). In Figure 4d, we show linecuts at 258 K, where two resonance features are resolved and fit by asymmetric Lorentzian lineshapes. The uniform mode (brown line) has a linear dispersion, however, the helical resonance (red line) has a constant resonance field from 4.5 – 5.5 GHz. The emergence of the helical resonance is more apparent in temperature scan in Figure 4e, showing that it gradually disappears as we approach the chiral ordering temperature. Moreover, we observe the helical resonance at both negative and positive fields (Figure 4f).

Due to the substrate-strain-induced uniaxial anisotropy in FeGe thin films, the magnetic moment tends to stay in the plane but twists along the substrate normal. The thickness of the film used in this study is 176 nm, which is 2.5 times of the FeGe helical vector of 70 nm. An in-plane magnetic field untwists the helical structure and forces into the field polarized phase. This behavior was observed in our magnetometry measurements, as well as previous MnSi thin film studies.

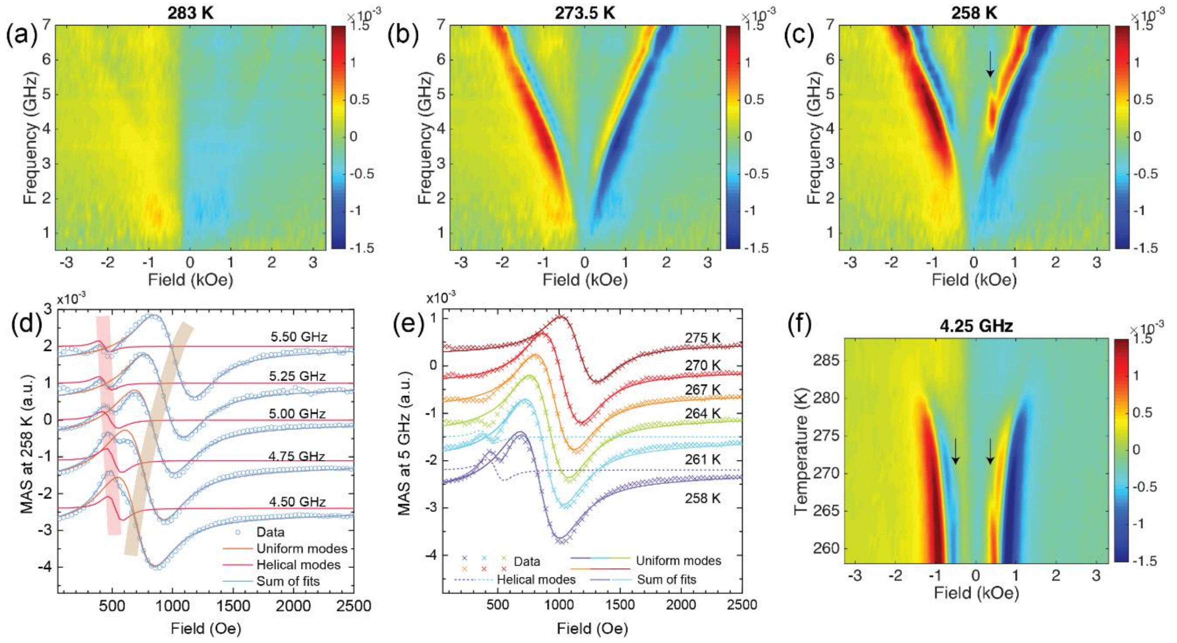

*Figure 4. Results of the microwave absorption spectroscopy. (a) Little absorption in paramagnetic phase at 283 K. (b) Only the field polarized resonance before the critical temperature at 273.5 K. (c) The helical and field polarized phase resonances at 258 K. (d) Line cuts at 258 K. The brown line shows the uniform mode,that follows Kittel's formula, the helical resonance is more independent of frequency which is shown by red curves. (e) Temperature scan line cuts. (f) Both positive and negative fields show helical resonances.*

To understand helical resonances more fully, we performed numerical micromagnetic simulations. We initialize the magnetic state of the film into a helix between 500 Oe and -500 Oe, and into a field polarized state at larger fields. These states are consistent with magnetometry measurements on our thin-film FeGe. After initialization, we relax the magnetic state to equilibrium at each field. We then apply a magnetic field impulse and analyze the natural oscillation frequencies of resulting magnetization dynamics. By calculating these natural frequencies at each field, we construct a power spectral density phase diagram as shown in Figure 5a, where we observe multiple resonance frequencies in the helical phases and the field polarized phase. We understand the resonances by dividing them into three regions: The uniform mode, shown at 1750 Oe as a function of thickness and frequency in Figure 5b, a spin helical mode, shown at 250 Oe with a 2.46

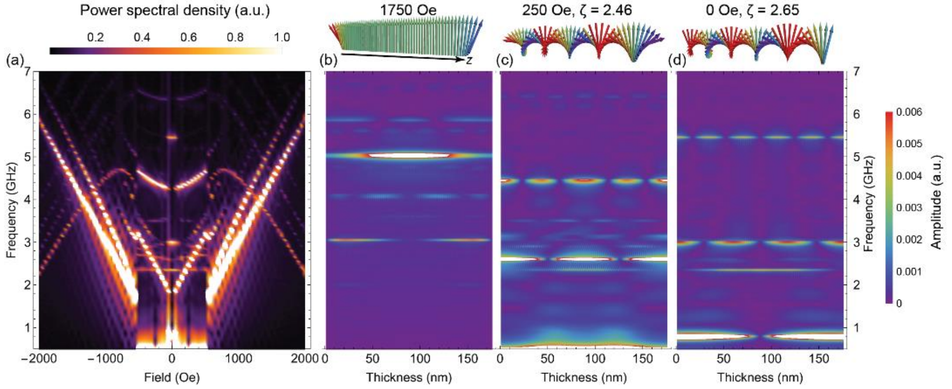

*Figure 5. Results of micromagnetic simulations of helical and field polarized spin textures. (a) Power spectral density plot shows resonance frequencies at corresponding magnetic field. The system is initialized as helix between 500 and -500 Oe fields and as field polarized at larger fields. (b) Uniform mode at field polarized phase. (c) Spin wave modes of helix at 250 Oe and (d) at 0 Oe fields. The winding number changes from 2.46 to 2.65, that passes the half-integer number, thus spin-wave node number changes from odd to even, which shows the sensitivity of spin-waves both the thickness and helical wave vector in chiral magnets.*

winding number shown in Figure 5c, and second helical mode, shown at 0 Oe with a 2.65 winding number shown in Figure 5d.

In the intermediate field case, there is a spin-wave resonance at 4.5 GHz, which is a close match to our experimental observations using MAS. In particular, the micromagnetic simulation reveals that spin-waves that match the helical wave number are resonantly enhanced in chiral magnets. At lower fields near zero, the winding number increases to 2.65 which causes the spin-wave mode to change from an odd to an mode because the winding number passed a half-integer (2.5) value, which further supports the correspondence between spin wave order and winding number. We conclude that spin-waves in chiral thin films are confined not only by the thickness, but also by the helical wave vector, which is a new mechanism controlling spin wave spectra.

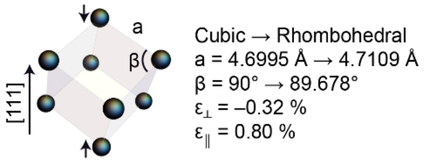

*Figure 6. Deformation of FeGe unit cell from a cubic into a rhombohedral. Out-of-plane and in-plane strains are found -0.32% and 0.8%, respectively.*

We characterized our sputtered films using x-ray diffraction (XRD), Transmission electron microscopy (TEM), and a scanning electron microscope equipped with electron back-scatter diffraction. We also measured the lattice spacing of FeGe along [111] and [400] indices by calibrating known values of Si substrate lattice constant. We found that our 176 nm thick FeGe film does not have truly cubic unit cell, it deforms into a rhombohedral unit cell. The quantitative deformation is shown in Figure 6. We find that our sputtered FeGe has 0.8 % tensile strain in-the-plane. Previously, it was believed FeGe adopts Si substrate lattice spacing and it has only 0.08 % strain. This is a key revelation because strain in FeGe introduces uniaxial anisotropy that suppresses the skyrmion phase of FeGe. Regardless of the claims, there have been no reports of skyrmions in FeGe grown on a substrate that have been validated by direct observation of skyrmions, either in a TEM or by neutron scattering. Therefore, by identifying the problem and finding a simple method to measure the strain in FeGe films on Si[111], we have a straightforward feedback mechanism to optimize scalable FeGe growth that does host skyrmions.

*Determining the phase diagram of FeGe using magnetic resonance*

During our spinwave study of FeGe thin films, we realized that (i) microwave absorption spectroscopy (MAS) is a very sensitive probe of magnetic phases, and (ii) there is no published research on the spin dynamics in bulk B20 FeGe to take as a reference so that we can understand the differences in thin films. Therefore, we undertook a study to systematically understand the microwave dynamics in single crystal FeGe, which has already been studied extensively using other methods including LTEM and neutron scattering. We obtained bulk FeGe crystals from Prof. Song Jin’s group at the University of Wisconsin–

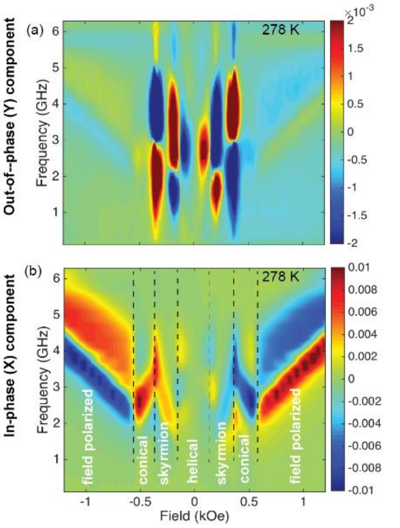

*Figure 7. MAS of single crystal bulk FeGe sample. Our first method is sensitive to the chiral phases in the out-of-phase component Y.*

Madison, where it is grown by chemical vapor transport. Using a simple set-up with an RF diode and lockin amplifier to record the transmitted microwave signal (Figure 3), we find remarkable sensitivity to the phase boundaries between magnetic phases (Figure 7). By varying the sample temperature, microwave frequency, and magnetic field, we establish the phase diagram of FeGe (Figure 8). We also performed micromagnetic simulations for all the spin texture to cross-check the observed spin resonances. We find that our phase map is in excellent agreement with previous neutron scattering experiments.

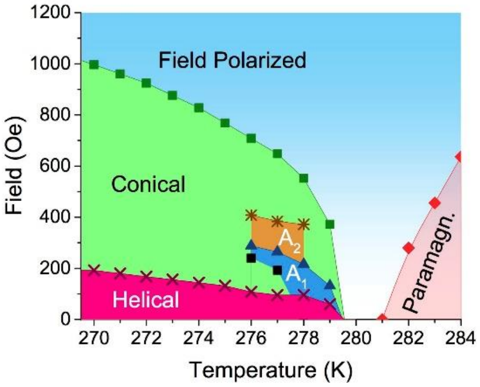

*Figure 8. Magnetic phase diagram of single crystal FeGe obtained by resonance spin dynamics as a function of temperature and magnetic field. Our phase diagram is in excellent agreement with previous neutron scattering experiments.*

## *Control of chiral spin textures through growth*

We also examined how to control the Dzyaloshinskii-Moriya interaction (DMI ) in thin films through stoichiometry, and thus tailor the helical pitch and skyrmion diameter. We chose to work with a solid solution of $Mn_xFe_{1-x}Ge$ because among the B20 materials, only this compound supports chiral magnetism for the entire range of *x* (between 0 and 1). As x varies, so does the helical period: theoretically ranging from infinity to 4 nm. This has previously been studied in polycrystalline bulk samples.

To co-deposit the three components, Mn, Fe, and Ge, we collaborated with Darrell Schlom to use his MBE system, which allows us to precisely control deposition rates and to monitor the crystallization process using an *in-situ* RHEED. This “during growth” feedback enables us to decrease the growth temperature down to 200 °C, which is critical because (as we learned in this study) the mismatch between the film and the Si substrate dominate the strain of the films. Therefore, by reducing the growth temperature, we were able to reduce the strain in MBE grown films by a factor of four times as compared to sputtered films. This is important because in-plane strain induces easy-plane magnetic anisotropy, which can eliminate skyrmion phase stability as we reported previously.

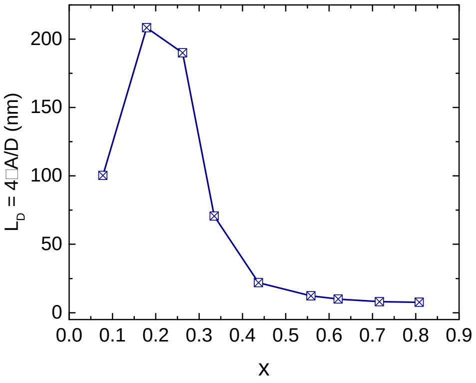

*Figure 9. Mn-concentration dependent helical period in MnxFe1-xGe thin films. We for the first time show a sub-10 nm helical period in a thin film.*

To extract the helical periods and DMI as a function of *x*, we perform dc magnetic characterization of the $Mn_xFe_{1-x}Ge$ films. We first measure the magnetization as a function of magnetic field, from which we find the saturation magnetization $M_s$ and the helical unwrapping field, $H_d$. We then apply a large magnetic field to saturate each film and measure the temperature-dependent magnetization, which follows Bloch-$T^{3/2}$ law due to thermal magnon excitations. From the Bloch-$T^{3/2}$ law, we extract the spinwave stiffness $D_{sw}$ and then find the symmetric and asymmetric exchange coefficients, A and D, respectively, in each film. The ratio of these two coefficient is proportional to the helical period $L_D$, which we plot in Figure 9. There is a critical concentration, $x_c \sim 0.20$, where DMI vanishes and the helical period approaches infinity. As Mn fraction $x$ increases further, the helical period starts to decrease again and it reaches 8 nm for the film with x = 0.81. We summarize the data we extract in Table 1.

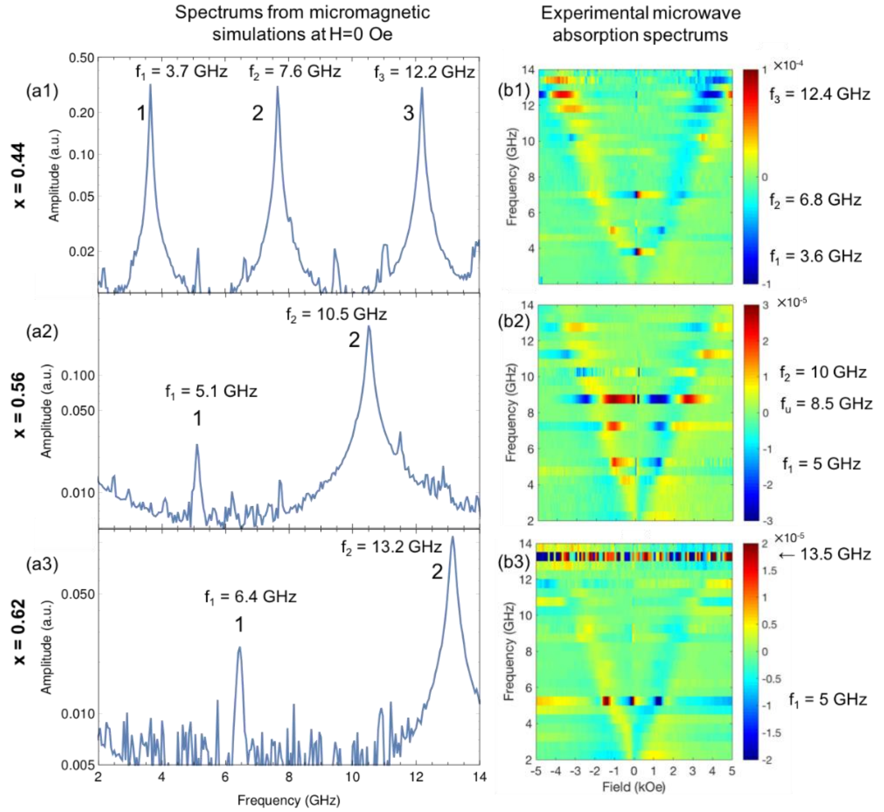

*Figure 10. Results of micromagnetic simulations and experimental MAS of helical spin textures for x=0.44, x=0.56, and x=0.62 Mn concentrations. The simulation spectrums are calculated at 0 Oe field in (a) and we focus on resonance features near zero field in (b). There are more resonances at non-zero fields; however, we are unable to understand their profiles at the moment.*

As verification of the helical textures, we also performed microwave absorption spectroscopy (MAS), which we modeled using micromagnetic calculations as shown in Figure 10. Our $Mn_xFe_{1-x}Ge$ films are 60 nm thick and not all the films have a full helical wrapping through the film thickness, thus not all are suitable for MAS measurements of the helical phases. Here we focus on three films with x =0. 44, 0.56, and 0.62. The first column of Figure 10 shows the simulated resonance spectra at 0 magnetic field, whereas and the second column shows MAS acquired as a function of magnetic field and frequency. Because we do not yet fully

*Table 1. Table 2. Physical and magnetic properties of $Mn_xFe_{1-x}Ge$ films. $\varepsilon_\perp$ and $\varepsilon_{||}$ are out-of and in-plane strains. We show the absolute values of DMI constants. Ms, A, and DMI are essential for the correct representation in micromagnetic simulations to account for the helical resonances.*

| Sample no. | Mn (%) | $\varepsilon_\perp$ (%) | $\varepsilon_\parallel$ (%) | $M_s$ (kA/m) | $H_d$ (kOe) | $L_D$ (nm) | $A$ (J/m $10^{-12}$) | DMI (mJ/m$^2$) |
|---|---|---|---|---|---|---|---|---|
| 1 | 0 | − 0.20 | 0.40 | 302 | 0.740 | 69.7 ± 3 | 1.37 ± 0.13 | 0.248 ± 0.026 |
| 2 | 7.8 | − 0.22 | 0.60 | 320 | 0.359 | 100 ± 5 | 1.47 ± 0.14 | 0.184 ± 0.019 |
| 3 | 17.9 | − 0.14 | 0.34 | 301 | 0.086 | 208 ± 11 | 1.43 ± 0.13 | 0.086 ± 0.009 |
| 4 | 26.2 | − 0.17 | 0.46 | 322 | 0.084 | 190 ± 10 | 1.24 ± 0.14 | 0.082 ± 0.010 |
| 5 | 33.5 | − 0.08 | 0.29 | 337 | 0.512 | 70.6 ± 5 | 1.09 ± 0.15 | 0.194 ± 0.029 |
| 6 | 43.7 | − 0.06 | 0.35 | 347 | 5.172 | 21.9 ± 1.5 | 1.09 ± 0.15 | 0.625 ± 0.096 |
| 7 | 55.8 | − 0.22 | 0.63 | 370 | 14.80 | 12.3 ± 0.9 | 1.06 ± 0.16 | 1.08 ± 0.18 |
| 8 | 62.1 | − 0.23 | 0.60 | 363 | 23.67 | 10.0 ± 0.7 | 1.10 ± 0.15 | 1.38 ± 0.21 |
| 9 | 71.6 | − 0.27 | 0.68 | 422 | 32.60 | 8.0 ± 0.6 | 1.13 ± 0.17 | 1.76 ± 0.30 |
| 10 | 80.8 | − 0.21 | 0.52 | 422 | 38.00 | 7.6 ± 0.5 | 1.19 ± 0.17 | 1.95 ± 0.31 |

understand the phase diagram of these films, we concentrate on the near-zero field resonances in which we know the films have a helical ground-state. Arrows in Figure 10 indicate semi-quantitative agreement between the simulation and experimental data, which strongly supports our understanding that the zero-field state is a helix and that our extracted magnetic parameters ($D$, $A$, $M_s$) are accurate.

This work is the first demonstration of epitaxial, phase-pure growth of B20 $Mn_xFe_{1-x}Ge$ thin films, which is exciting because these films represent a model-system to study basic physics and the device integration of sub-ten nm Bloch magnetic skyrmions. As such, thin film versions of DMI-controllable $Mn_xFe_{1-x}Ge$ thin films could play a curial role in developing devices and prototype technology. This includes high-density, low power memory and logic technologies. Additionally, these materials have potential applications in frequency tunable spin-torque oscillators using chiral magnets.

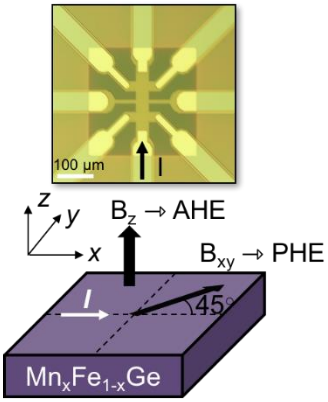

*Figure 11. Top image shows a fabricated Hall device and the bottom image shows an experimental schematic for measuring the Anomalous and Polar Hall effects and magnetoresistance.*

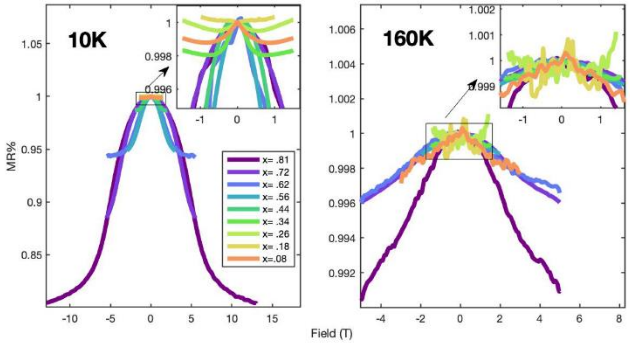

*Figure 12. Longitudinal resistivity with out-of-plane applied field. $\rho_{xx}$ measurements at 10 K and 160 K are plotted vs. out-of-plane applied field, $H_z$. Resistivity for each plot is normalized by $R_0$, the resistivity at $H_z$ = 0. x is the Mn concentration in $Mn_xFe_{1-x}Ge$.*

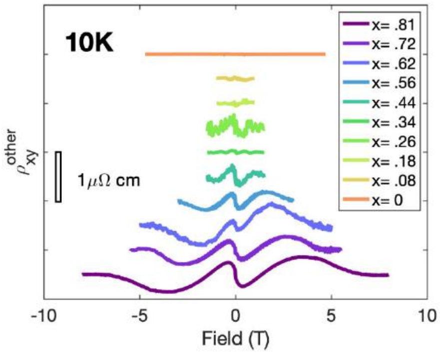

*Figure 13. Extracted THE at 10K for all samples. Obtained by finding the difference between measured Hall resistivity and the sum of the OHE and AHE. Nonzero THE is evidence of a contribution to the Hall effect from something in addition to the ordinary and anomalous contributions.*

One critical open question in the field of topological magnetism is: why are theoretical predictions for the topological Hall effect orders of magnitude different than experiments in both Néel and Bloch skyrmion materials? Furthermore, even the anomalous Hall effect in these materials are poorly understood. Nonetheless, these effects are integral to connection between spin-orbit interactions, Berry's phase, and DMI. Our $Mn_xFe_{1-x}Ge$ thin films will be valuable for investigating this problem because we can systematically control both DMI and device geometry and observe the resulting Hall and magnetoresistance effects.

In Figure 11, we show an example device and schematic of the experimental geometries. Here, we show the longitudinal resistivity in Figure 12, which displays anisotropic magnetoresistance (AMR). The films with $x = 0.08$ Mn fraction show only 0.1% AMR, which is typical for ferromagnets (e.g. Co, Fe and their alloys); however, the film with $x = 0.81$ shows 13% AMR, which is surprisingly large and potentially significant for applications in chiral materials.

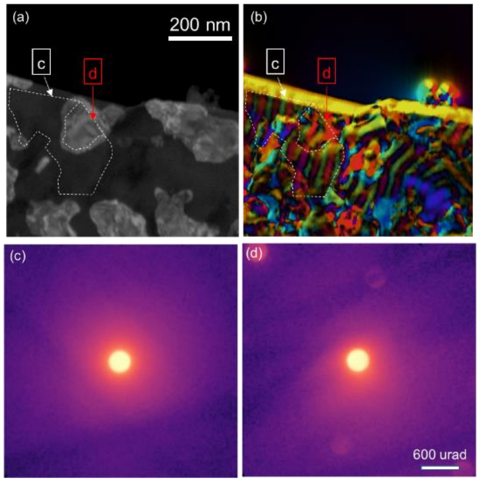

*Figure 14. By analyzing the grain orientations shown in the ADF image (a) and we relate it to the magnetic field image in (b), we realized that adjacent grains c and d have a generalized grain orientation.*

In Figure 13 we show the "other" Hall effect that is obtained by separately measuring the ordinary and anomalous Hall contributions and subtracting them from $\rho_{xy}$, the total Hall effect resistivity. This has often been interpreted as a topological Hall effect, which remains controversial for these materials. Based on our magnetic characterization and the known easy-plane anisotropy, we know that there are no skyrmions in these films giving rise to a topological Hall effect (THE). On the other hand, these materials are highly chiral, and a result disordered magnetic states can contribute fractional topological textures that are broken by grain boundaries with opposite chirality. This may be the origin of an apparent THE signal in these materials even if there are no skyrmions.

*Disentangling grain and magnetic texture in electron microscopy*

In collaboration with David Muller's group at Cornell, we used Lorentz scanning electron microscopy to with a pixel-array detector (EMPAD) to distinguish between magnetic and structural contrast. One puzzle we encountered at the time is that the helical wave-vector shifts at phase boundaries (Figure 14). Using EMPAD measurements, we were able to extract the chirality of grains and the sign of the local DMI. For comparison, we performed micromagnetic simulations of random grains, with randomly assigning DMI signs. In agreement with the experimental observation, we found that helical vectors shift in space to adjust them for the opposite DMI sign (Figure 15). This brings out important questions of skyrmion phases and dynamics in twinned B20 thin films and sets a goal to increase grain sizes by engineering interfaces with better seed layers on which B20 films grow.

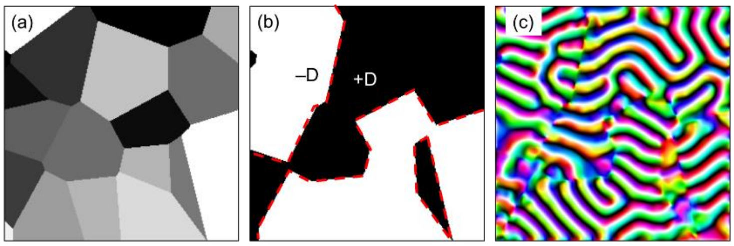

*Figure 15. Micromagnetic simulations of a disordered FeGe film to demonstrate spatial shift of helical wavevector through grain boundaries, which have opposite sign DMI coefficients. (a) Randomly generated grains, (b) assigned the opposite signs of DMI coefficient, (c) resulting ground state spin texture, in which color code represents magnetization orientation. The simulation window is 1024x1024 nm2.*

Subsequently, we have tried to grow untwinned FeGe and FeMnGe using both sputtering and MBE by varying the substrate, underlayers, introducing interface DMI with Pt interfaces, and several other things, and none of them were successful. This remains an outstanding challenge for useful technology taking advantage of the strong intrinsic chirality of B20 thin films.

**List of Papers:**

1. E. Turgut, A. Park, K. Nguyen, A. Moehle, D. A. Muller, and G. D. Fuchs, "Chiral magnetic excitations in FeGe films." *Phys. Rev B* **95**, 134416 (2017). https://doi.org/10.1103/PhysRevB.95.134416
2. E. Turgut, M. J. Stolt, S. Jin, and G. D. Fuchs, "Topological spin dynamics in cubic FeGe near room temperature." *J. Appl. Phys.* **122**, 183903 (2017) https://doi.org/10.1063/1.4997013
3. E. Turgut, H. Paik, K. Nguyen, D. A. Muller, D. G. Schlom, G. D. Fuchs. "Engineering Dzyaloshinskii-Moriya interaction in B20 thin film chiral magnets" *Phys. Rev Mater*. **2**, 074404 (2018). https://doi.org/10.1103/PhysRevMaterials.2.074404
4. Kayla X. Nguyen, Emrah Turgut, Michael C. Cao, Jack Glaser, Zhen Chen, Matthew J. Stolt, Song Jin, Gregory D. Fuchs, and David A. Muller, "Disentangling magnetic and grain contrast in polycrystalline FeGe thin films using 4-D Lorentz Scanning Transmission Electron Microscopy." arXiv:2001.06900 (2020).